



Sediment loss modelling framework for the Bradano River Basin, southern Italy, 1950–2020

Nazzareno Diodato¹ · Pasquale Borrelli² · Iñigo Gómara³ · Gianni Bellocchi^{1,4}

Received: 25 March 2022 / Accepted: 16 September 2023 / Published online: 2 October 2023
© The Author(s) 2023

Abstract

Hazardous hydrological events cause soil erosion and it is essential to anticipate the potential environmental impacts of prevailing erosion processes that occur at different time-scales. Here, we present the modelling of net soil erosion rates for the Bradano River Basin (southern Italy), based on rainfall erosivity, surface overland flow and transport sub-models. A semi-empirical framework was developed, upscaling point rainfall values based on the Foster-Thornes approach in order to give an insight into monthly and annual soil losses over the period 1950–1958 and 1961 (calibration) and over a longer time-frame (1950–2020: reconstruction). In the 2765-km² study area, ~68% of the sediment mobilized within the basin reached the basin outlet (mean value for 1950–2020: ~366 Mg km⁻² yr⁻¹). A moderate declining trend in net erosion rates was observed after the 1980s, concurrent with the contraction of cropland in favour of natural vegetation and river channelization. Our results suggest that the parsimonious principle used here seems sufficiently robust to be suitable for applications in other Mediterranean landscapes.

1 Introduction

Accelerated soil erosion has substantial implications for nutrient and carbon cycling (Ran et al. 2018), sustainable land productivity and socio-economic development (Browning and Sawyer 2021). Mediterranean areas are particularly affected by soil loss by water erosion and displacement of sediment (Diodato et al. 2021b). Already

the empirical observations of the Italian High Renaissance polymath Leonardo da Vinci (1452–1519) in his *Trattato sull'acqua* (“Treatise on Water”), published in 1489, showed the interaction between rainfall and landscape in determining soil erosion (Cardinali 1828).

In recent decades, important progress has been made in understanding, describing and modelling soil erosion at different spatial scales (de Vente et al. 2013). However, the timescale (from months to decades) has received less attention because monitoring of climate, hydrological and erosional processes are mostly not available for extended periods (Kemp et al. 2020). A wide range of models are available to attempt to simulate the intricate dynamics in soil gross and net erosion (Borrelli et al. 2021).

The Universal Soil Loss Equation (USLE) of Wischmeier and Smith (1978) and the Revised Universal Soil Loss Equation (RUSLE) were developed in the early 1990s (Renard et al. 1991). The latter is the most widely used model for assessing erosive soil degradation (e.g. Van Rompaey et al. 2001; Pruski and Nearing 2002; Jiang et al. 2012). Other useful models for predicting soil erosion dynamics include the Watershed Erosion Prediction Project (WEPP) by Guo et al. (2021), the Water and Tillage Erosion Model and Sediment Delivery Model (WATEM/SEDEM) by Borrelli et al. (2018) and the Soil and Water Assessment Tool (SWAT) by Hussainzada and Lee (2022). Under the

✉ Iñigo Gómara
i.gomara@uva.es
Nazzareno Diodato
scodalabdiodato@gmail.com
Pasquale Borrelli
pasquale.borrelli@unipv.it
Gianni Bellocchi
gianni.bellocchi@inrae.fr

¹ Met European Research Observatory, International Affiliates Program of the University Corporation for Atmospheric Research, 82100 Benevento, Italy
² Department of Earth and Environmental Sciences, University of Pavia, 27100 Pavia, Italy
³ Departamento de Matemática Aplicada, Escuela de Ingeniería Informática, Universidad de Valladolid, 40005 Segovia, Spain
⁴ Université Clermont Auvergne, INRAE, VetAgro Sup, 63000 Clermont-Ferrand, France

condition of scale invariance (over time) of topographic and lithological factors, soil losses mostly depend on the rainfall erosivity and vegetation cover. Thus, quantifying the effects of climate change-induced variations on erosivity and land use changes on soil protection is important to identify critical areas prone to soil erosion (Gupta and Kumar 2017). For that, such complex approaches require many factors that are not always readily available for long-term estimates, and the application of such models can be challenging due to data availability issues (Merritt et al. 2003). Consequently, these models may not fully capture the occurrence and co-evolution of natural phenomena mechanisms across various timescales (Zhang et al. 2001). Despite these limitations, they can still serve as valuable tools in complementing empirical observations to support sustainable landscape management (Arabameri et al. 2021). Recent satellite development and data applications have also provided a better understanding of how natural and anthropic changes are evolving, and how they influence landscape dynamics. However, also in this case, only short time-series are available (Cudahy et al. 2016). To reconstruct inter-annual and inter-decadal variability in the evolution of landscape responses over several decades in historical times, a simpler approach using only monthly and daily rainfall amounts is preferable. Conceptual and regression-derived erosion models offer a parsimonious interpretation of the relationships between input data and basin-responses on the assumption of a homogeneous basin unit and can thus be more easily adopted (de Vente and Poesen 2005). However, parsimony is a prerequisite for model building and facilitates its use, not an indication that nature operates on the basis of parsimonious principles (Mulligan and Wainwright 2004). Semi-empirical models, based on simple physical concepts, are far more interesting from an interdisciplinary point of view because they can appeal to a wide range of scientists and end-users, who can communicate more easily than with physically-based models. In fact, this has stimulated the identification of concepts for the development of parsimonious modelling solutions for the assessment of sediment loss in river systems (Gericke and Venohr 2012; Diodato et al. 2012, 2015, 2018, 2022; Diodato and Bellocchi 2019).

In recent decades, geomorphological studies that have considered Basilicata Region, in southern Italy (Pilogallo et al. 2020), and in particular the Bradano basin, have focused on the long-term annual mean estimation of soil erosion (Spilotro et al. 2010; Aiello et al. 2015), yet leaving inter-annual dynamics unexplored. These temporal scales are important for the study of soil erosion because within them extreme events can occur and significantly alter the perception of erosive hazard that is hidden when only a mean value is estimated (Kinnel 2010).

Basilicata is one of the most hydrologically vulnerable regions in Italy (Gostelow et al. 1997). For instance, the Bradano River Basin (BRB) has been recently affected by extreme rainfall events, such as the one inducing the flood of 1 March 2011 (with 90 mm d^{-1}), and those of an exceptional nature that occurred within about two months of each other: the event of 5–7 October and those of 1–2 December 2013. The first affected the province of Matera (in the south-east) and caused serious and widespread damage in many parts of its territory, including floods in the basins of Bradano and Basento rivers and occurrence of numerous landslides and soil erosion phenomena. The second occurred in early December, with violent rainstorms in the Metapontino area (in the lower part of the BRB), with rainfall accumulated between 1 and 2 December 2013 up to values above 150 mm, with peaks of 200 mm (Manfreda et al. 2015). The latest floods with accelerated erosions occurred on 12 November 2019 and mainly affected the south-eastern part of the BRB around Matera.

However, rainfall-induced slope failures and erosion are not new phenomena in Basilicata. Already between the end of the 18th century and the first half of the 19th century, many lands of Basilicata were ploughed and cultivated, hundreds of hectares of woodland were cleared, and so often they were affected by remarkable erosive processes, as the contemporary historian Piero Bevilacqua wrote (Labella 2010, p. 17):

“le alture diboscate, e in primissimo luogo le terre di pendio, private della più o meno antica copertura forestale, erano sottoposte a intensi processi di erosione del suolo [con] smottamenti di terre e frane [...] che investivano talora interi paesi posti a valle, colture, strade [...]. Il diboscamento delle terre di altura produceva alterazioni di grande portata perché i torrenti, costretti a trascinare a valle massi e detriti”

“the cleared hills, and in the first place the lands of slope, deprived of the more or less ancient covering forestry, were subjected to intense processes of soil erosion [with] landslides [...] which sometimes affected entire villages downstream, crops, roads [...]. The deforestation of highlands produced far-reaching alterations because the streams, forced to drag downstream boulders and debris”

The winter floods overflowed and widened the riverbeds to form widespread swamps and marshes near the mouth of the rivers. In these dynamic and sensitive landscape systems driven by climatic, geomorphic and ecologic processes, and where magnitude of events is nested in longer-term environmental factors, the use of modelling to support the assessment of water erosion is a challenge (Thomas 2001). With focus on the BRB, given the issue of assessing erosive sediment by complex models in recognition of the detailed input for the

historical period, we arranged a parsimonious erosion model adapted to the monthly and annual scales from the original algorithms of Foster et al. (1977) and Thornes (1990), because they provide an interpretation of empirically determined factors shaping active erosional landscapes in basin areas based on the parsimonious balance between driving and resisting forces in the sediment budget. In particular, the goal of this study was to develop a monthly based parsimonious erosion model, REgression-Derived Erosion Model – REDEM_(BRB) for the BRB. The model aims to estimate soil erosion based on factors such as runoff, slope gradient, soil erodibility (driving forces) and vegetation cover (resistance force). By generating a long erosion time-series from 1950 to 2020, the study seeks to explore geomorphological processes in this Mediterranean river basin.

2 Material and methods

2.1 Study area

The study area covers 2765 km², of which 2010 km² belong to the Basilicata region and the remaining 755 km² to the Apulia region. In the Italian context, this area is affected by moderate to strong soil erosion (Fig. 1a). The river Bradano (about 120 km long) starts from the Apennine chain on the northwest side of the river basin and reaches the Ionian Sea, with its mouth at Tavole Palatine (Fig. 1b). The basin has a mountainous morphology only in the north-western

and northern areas, with altitudes between 700 and 1250 m a.m.s.l. The NW–SE strip of territory between Forenza (40° 52' N, 15° 51' E) and Spinazzola (40° 58' N, 16° 05' E) to the north, and Matera (40° 40' N, 16° 36' E) and Montescaglioso (40° 33' N, 16° 40' E) to the south is characterised by hilly morphology with altitudes between 300 and 500 m a.m.s.l. The north-eastern sector of the basin includes part of the inner margin of the *Altopiano delle Murge* (Murge plateau), which has shares varying between 400 and 600 m a.m.s.l. The mean slope is about 12%, and 8% of the area has a slope of over 30% (Canora et al. 2015).

According to the classification plan of the Basilicata region (<http://www.bradanometaponto.it/PianoClassifica.html>), the landscape is dominated by arable non-irrigated lands. The utilised agricultural area (UAA) of over 218,000 ha accounts ~85% of the total farm areas, and the types of production are mainly wheat, olives, citrus and fruit crops. Cereal cultivation is the most widespread (~48% of the UAA), with durum wheat (a subsidised crop) playing a predominant role, accounting for ~95% of the cereal area. As far as olive growing is concerned, the area is particularly suited to this type of production, covering an area of ~16,000 ha (~7% of the UAA). In coastal areas, the agro-pedological nature of the land and the favourable climatic conditions allow the establishment of more profitable crops, such as fruits and vegetables (i.e. tomatoes, strawberries, oranges, lemons, tangerines, clementines, peaches and apricots), thanks also to a well-structured irrigation network. The hills are characterised

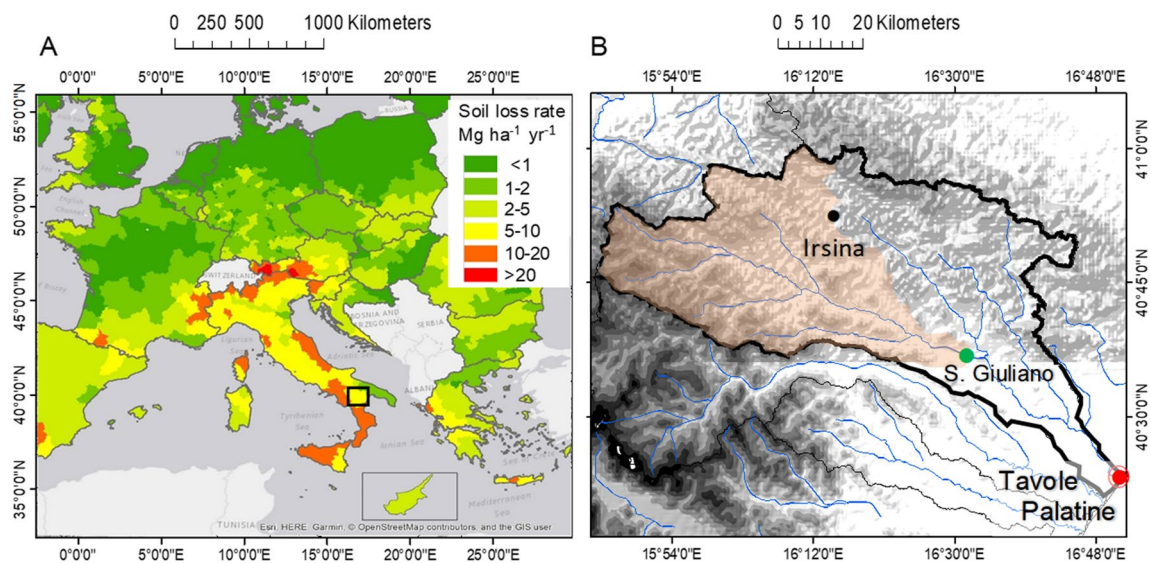


Fig. 1 **A** Map of the mean rate of soil loss in central and southern Europe; **B** hydrographic network of the Bradano River Basin with the basin outlet (red dot) at the hydrometric station of Tavole Palatine (40° 24' N, 16° 49' E), the sub-basin (light brown) subtended by the San Giuliano (40° 36' N, 16° 29' E) dam (green dot) and the reference pluviometric station (black dot) of Irsina (40° 45' N, 16°

14' E). The black square in **A** identifies the study region (Basilicata). The data in **A** were arranged from the European Soil Data Centre (ESDAC, <https://esdac.jrc.ec.europa.eu/themes/rainfall-erosivity-europe>); adapted from Panagos et al. 2020). The graph in **B** was arranged from the Italian Institute for Environmental Protection and Research (<http://sgi2.isprambiente.it/viewersgi2>)

by patches of cultivated landscape. The percentage of surface area covered by woods is highly inhomogeneous in the municipalities that fall within the basin. Forests are mainly present at the highest elevations of the north-western part of the basin, along the Apennine ridge. Pastures and meadows cover an area of ~19%, with sheep and goat farms widespread throughout the area (mainly the Murgian plateau), where significant livestock activities are mostly conducted on a pastoral basis. Towards the south, the natural vegetation becomes that typical of the Mediterranean maquis. Coniferous plantations are present inland and along the coast. Along the hydrographic network, hygrophilous vegetation is predominant (Aiello et al. 2015).

The soils of the rough mountains are formed on a substratum of flyschoid sedimentary rocks, while the soils of the clay hills, which extend from the north of the central area to the south, in the immediate vicinity of the Ionian Sea, consist of fine-grained clay-silt marine deposits (Canora et al. 2015).

The climate is typically Mediterranean (Köppen-Geiger Csa), characterised by cool to mild, wet winters and warm to hot, dry summers. The winter season is mainly between October and February, when precipitation is dominated by the passage of synoptic low-pressure systems (Hawcroft et al. 2012). In the southern and coastal part of the basin, summers can often be similar to those of arid and semi-arid climates, where long periods with little rainfall are interrupted by heavy erosive convective precipitation (Fig. 2a). The spatial pattern of mean annual rainfall erosivity in the BRB ranges

from 700 to 1200 MJ mm ha⁻¹ h⁻¹ yr⁻¹ (Fig. 2b), and is concentrated in summer and early autumn, when the soil is more susceptible to erosion (Fig. 2a, red empty histogram). However, rainfall erosivity (i.e. the potential of rainfall to cause soil erosion) shows considerable inter-monthly variability and at same time a multi-modal distribution, with hazard values between summer and early autumn, when the soil begins to be free of vegetation. It also shows an intra-seasonal cycle decoupled from the rainfall regime.

2.2 Data and conceptual scheme

Net erosion, also known as sediment yield, is the sum of sediment produced by all sources of soil erosion, including from splash erosion, overland flow and runoff, and stream channel areas, minus the amount of sediment deposited in these areas and in valley floodplains, which cross the outlet of a river basin (e.g. Toy et al. 2002). For this study, we have referred to the rainfall and net erosion data provided by the Regional Agency for Environmental Protection of Basilicata (ARPAB, *Centro Funzionale Protezione Civile*, <http://centrofunzionalebasilicata.it>). For the BRB, net erosion data are available for the years 1950–1958 and 1961 (Annals Project of the former Hydrographic and Mareographic National Service, 1957–1972, <https://www.isprambiente.gov.it/it/progetti/cartella-progetti-incorso/acque-interne-e-marino-costiere-1/progetti-conclusi/progetto-annali>), which were used for the calibration of the erosion model. The Irsina rainfall station (Fig. 2b),

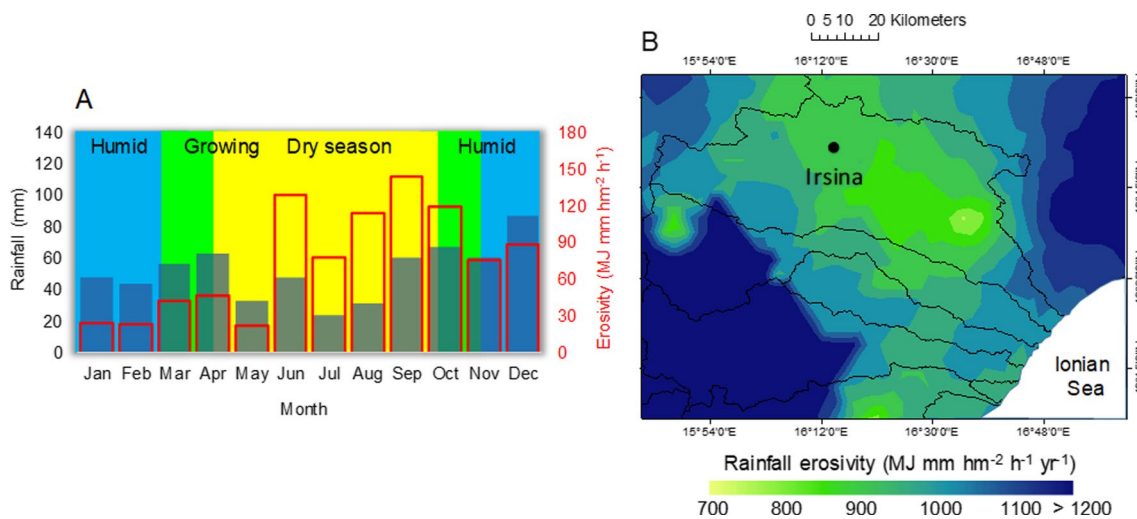


Fig. 2 **A** Monthly precipitation (solid bars) and rainfall erosivity (red blank bars) for Irsina station, and **B** spatial pattern of annual rainfall erosivity across the Bradano River Basin averaged over the period 2001–2011. In **A**, rainfall data from SCIA (*Sistema nazionale per l'elaborazione e diffusione di dati climatici*) dataset (<http://www.scia.isprambiente.it>) for the period 1971–2010 were arranged by FAO LocClim software (<https://www.fao.org/land-water/land/land-gover>

[nance/land-resources-planning-toolbox/category/details/en/c/1032167](https://www.fao.org/land-water/land/land-governance/land-resources-planning-toolbox/category/details/en/c/1032167)) on rainfall data from 1971 to 2010, while rainfall erosivity data were derived from Capolongo et al. (2008) for the period 2001–2005. In **B**, ESRI-ArcGIS Gaussian interpolation was performed by the European Soil Data Centre (ESDAC, <https://esdac.jrc.ec.europa.eu/themes/rainfall-erosivity-europe>; Panagos et al. 2017)

located at 548 m a.m.s.l., is the only one in the basin area that provides a continuous daily rainfall time-series for a long period, i.e. 1950–2020, which was used for model calibration and reconstruction of net erosion. Monthly data of vegetation cover are not available before 1981. Until 1980, the monthly vegetation cover percentage (VCP) was parameterized annually on a constant basis, with a monthly variation from January to December. The vegetation cover data up to 1980 were thus obtained by calibration of the model. Subsequently (until 2020), variable values were obtained over the BRB based on actual Normalized Difference Vegetation Index (NDVI) data from NOAA Climate Data Record (Vermote 2019), provided by Climate Explorer at a resolution of 0.1° (cell data over $\sim 10 \text{ km} \cdot 10 \text{ km} = 100 \text{ km}^2$). The annual NDVI values assigned to the BRB were the mean of the gridded data-points in (and around) the area of interest (i.e. 28 pixels). We had to transform NDVI values into VCP (%), since the model we developed — Eq. (1) — includes the exponential vegetation function of Thornes (1990), which is based on VCP. Since NDVI and VCP were only available simultaneously for the year 1981, we had to develop a ratio between VCP and NDVI so that we could use it to estimate VCP over the entire period covered by NDVI. In 1981, the ratio between the VCP and NDVI was calculated for each month (from January to December): 80, 48, 50, 36, 53, 158, 179, 201, 153, 120, 115 and 122. These values likely reflect the agrarian landscape of previous years in Basilicata, which only saw significant transformations in the late 1970s (Giambersio and Menchise 2010). From 1982 onwards, this ratio was used to estimate the VCP by multiplying it by NDVI. Daily E-OBS (<https://www.ecad.eu/download/ensembles/download.php>) gridded precipitation data at 0.25° horizontal resolution (cell data over $\sim 25 \text{ km} \cdot 25 \text{ km} \approx 625 \text{ km}^2$) for the period 1950–2020 (Cornes et al. 2018) were also considered in the study (i.e. areal mean of nine nodes at the crossing points of 12 pixels, four of which falling entirely within the basin).

These erosional features are thus taken into account in a hierarchical structure to discover the erosional phenomena in the present time. In this way, the temporal changes in water-driven soil erosion are influenced by both short-term convective storm events and longer-term environmental and climatic variations occurring at different time scales (Thomas 2001). However, using the procedure originally developed by Wischmeier and Smith (1965) to estimate mean annual erosion may not accurately capture soil loss from individual storms or monthly data (Haan et al. 1994). To address this limitation, Foster et al. (1977) suggested a modified approach suitable for individual storms or monthly data. In Italy, historical monitoring of rainfall and sediment yield provided the basis for adapting and calibrating the Foster-Thornes' algorithm into a semi-empirical erosion

model, here called REDEM (REgression-Derived Erosion Model). In this model, the driving forces are simplified into rainfall and runoff proxies or indicators, representing splash and transport erosion, respectively. The model incorporates seasonal effects, considering the interaction between rainfall erosivity and the varying soil erodibility conditions during different seasons (Diodato and Bellocchi 2019; Diodato et al. 2022).

The parameterization of the model was derived from physical and statistical considerations that were integrated with observed correlations, and included the upscaling issue through both the exponent of dx term in Eq. (2) and the exponential vegetation function of Thornes (1990). The gridded time-series of dx (0.25° spatial resolution) are too coarsely resolved to allow a reliable estimation of soil erosion from precipitation patterns. Here, we use basin-wide dx values, upscaled from the high-quality daily maximum rainfall data available monthly from a single station in the basin (monthly hourly data are not available). In particular, we applied a trigonometric approach, which is typically implemented to represent cyclical processes (including intra-seasonal climatology), as documented for instance, in Diodato and Bellocchi (2007a, b) and Diodato et al. (2021a). For site-to-basin area upscaling, we refer to Diodato et al. (2017). The mathematical formulation of the process studied, developed at a point-station, was thus designed to be representative over an area as large as a homogeneous basin unit, as follows:

$$\text{REDEM}_{(\text{BRB})} = A \cdot [(R_S + R_Q) \cdot e^{-0.07 \cdot \text{VCP}}] \cdot \text{SDR} \quad (1)$$

where $\text{REDEM}_{(\text{BRB})}$ is the modelled net erosion in $\text{Mg km}^{-2} \text{ month}^{-1}$, A is a parameter of scale that depends on geographical characteristics of the basin; R_S is the rainfall-erosivity indicator associated more to splash erosion and rill erosion; R_Q is the erosivity indicator linked more to overland flow and transport erosion; $e^{-(0.07 \cdot \text{VCP})}$ is the exponential Thornes's (1990) vegetation function, with the vegetation cover percentage (VCP) at contact with the surface; in fact, we can assume in first approximation that, surfaces hydraulically rough and covered from plants, reduce flow velocity and hence soil interrill transport capacity (Toy et al. 2002). This fraction (%) was set constant until 1980, and subsequently variable, until to 2020, accordingly with the NDVI actual data as described above.

As canopy cover reduces the erosivity of raindrop for detachment, it also reduces interrill sediment-transport capacity. The last component of the model is the sediment delivery ratio (SDR), which is the sediment yield from the catchment area divided by the gross erosion (GE) of that same area. Expressed as a fraction, it represents the efficiency of the catchment in moving soil particles from areas of erosion to the

point where sediment yield is measured. Including SDR as an explicit variable in the model allows for the consideration of factors other than vegetation cover that influence runoff and its peak, such as basin shape, relief-length ratio, soil texture, the transport process and the gradient of the main channel slope (e.g. Van Rompaey et al. 2001). Based on this understanding, rainfall power as the prevailing storm erosivity in summer and autumn is mainly captured by the R_S term (unitless), while in winter and spring, runoff is mainly captured by the R_Q term (unitless). In this way, soil erosion by water occurs more when the detachment of particles and their subsequent transport experience a greater driving force than the force that binds it into the vegetated slope. Within these processes, rain is used by nature as both a driving and resisting factor. Firstly, the erosive influence of rainfall increases with its amount, intensity and runoff; secondly, and in opposition to this influence, it is the protective effect of vegetation that also increases with the amount of rainfall.

Explaining the single terms, we obtained, arranging from Diodato and Aronica (2014):

$$R_S = (1 + dx^\theta) \cdot \left[1 - \Omega \cdot \cos \cdot \left(6.28 \cdot \frac{j - \sigma}{\varphi - j} \right) \right] \tag{2}$$

where dx is the maximum daily rainfall (mm d⁻¹) in each j month, the term in brackets is a site-to-basin scale transfer function including the unitless upscaling parameter θ , and the term in square brackets represents the periodic function including the unitless scale factor Ω , as well as the unitless position parameters σ and φ . These parameters are used to modulate the amplitude of intra-seasonal rainfall intensities, reflecting the distribution of maximum hourly rainfall over the year. This is in agreement with a multivariate analysis that explained how the inclusion of the effect of rainfall intensity increases sediment yield by ~24%, compared to the most notable single factor, i.e. rainfall duration (Shojaei et al. 2020).

The following R_Q term represents, instead, an erosivity indicator more associated with runoff-driven erosion:

$$R_Q = p \cdot \left[\alpha + \beta \cdot \cos \left(6.28 \cdot \frac{j}{\omega - j} \right) \right] \tag{3}$$

where p is the amount of rainfall (mm) in each month j ; the term in brackets is an indicator of soil humidity as a periodic function (with three empirical, unitless parameters α , β and ω) to modulate the intra-seasonal humidity after precipitation. This relies on Zhang et al. (2017), who found that surface conditions on the loess slope significantly affected runoff and sediment yield processes, which is of great significance to further summarize the relationships between runoff and sediment yield, and to

understand the variation in sediment yield associated with different rainstorms.

Based on Arnold et al. (1995), the sediment delivery ratio (SDR) was estimated as (with ψ and η empirical parameters):

$$SDR = \left[\psi \cdot \left(0.78 + 0.22 \cdot \frac{R_Q^\eta}{1 + p} \right) \right]^{0.56} \tag{4}$$

The concept is an analogue to the connectivity ratio (the amount of sediment reaching an outlet over the amount of sediment eroded), which characterises the efficiency of slope-channel transfer and depends on the transport capacity and slope-shape and drainage pattern (e.g. Quinton et al. 2006).

Once net erosion (NE) is estimated using Eq. (1), from simplifying the mass-balance equation that describes the variables that define NE (Toy et al. 2002), it follows:

$$NE + D = \frac{NE}{SDR} \tag{5}$$

with deposition sediment within the basin (D) as:

$$D = NE \cdot \left(\frac{1}{SDR} - 1 \right) \tag{6}$$

By replacing NE with Eq. (1), we obtained:

$$D = A \cdot \left[(R_S + R_Q) \cdot e^{-0.07 \cdot VCF} \right] \cdot SDR \cdot \left(\frac{1}{SDR} - 1 \right) \tag{7}$$

2.3 Model parameterization and evaluation

The modelling procedure was carried out on 120 monthly sediment data (included in the period 1950–1958 and 1961) by iteratively adding predictors and comparing the model predictions with the observational data. The parameters A in Eq. (1), θ , Ω , σ and φ in Eq. (2), α , β and ω in Eq. (3), and ψ and η in Eq. (4) were calibrated through a trial-and-error process. Previous studies with similar modelling approaches informed our calibration process (e.g. Diodato and Bellocchi 2019). The calibration aimed to establish a significant relationship between actual and predicted data, ensuring that the following criteria were met (Diodato et al. 2020):

$$\begin{cases} R^2 = \max \\ MAE = \min \\ |b - 1| = 0 \end{cases} \tag{8}$$

i.e. maximizing the goodness-of-fit (R^2 , optimum 1), minimizing the mean absolute error (MAE, optimum 0) and minimizing the difference from the unity of the regression

slope (b , optimum 1) between actual and modelled data. An efficiency metric, the Nash–Sutcliffe index ($-\infty < EF \leq 1$, optimal) was also calculated to assess model performance uncertainty, as $EF > 0.6$ indicates narrow parameter uncertainty (Lim et al. 2006). The Durbin–Watson statistic was also performed to check for the presence of autocorrelated residuals, as strong temporal dependence can induce spurious correlations.

Statistical analyses were spreadsheet-based with the support of software STATGRAPHIC (<http://www.statpoint.net/default.aspx>), CurveExpert Professional 1.6 (<https://www.curveexpert.net>), WESSA (<https://www.wessa.net/tsa.wasp>) and MATLAB® (<https://www.mathworks.com/products/matlab.html>).

3 Results and discussion

3.1 Model parameterization and evaluation

A highly significant relationship ($p < 0.01$) was obtained between the available sediment data for the years 1950–1958 and 1961, and the corresponding predictions using the following calibrated parameter values: $A = 2.19$ in Eq. (1), $\vartheta = 2$, $\Omega = 0.60$, $\sigma = 4$ and $\varphi = 19.6$ in Eq. (2), $\alpha = 0.4$, $\beta = 0.2$ and $\omega = 25$ in Eq. (3), $\psi = 0.5$ and $\eta = 1.3$ in Eq. (4). Additionally, the calibrated monthly variation of the vegetation cover percentage (VCP) was as follows: 25% in January, 15% in February, 21% in March, 20% in April, 30% in May, 55% in June, 55% in July, 55% in August, 45% in September, 35% in October, 32% in November and 31% in December. These calibrated values reflect the distribution pattern of mean monthly values for the years 1950–1958 and

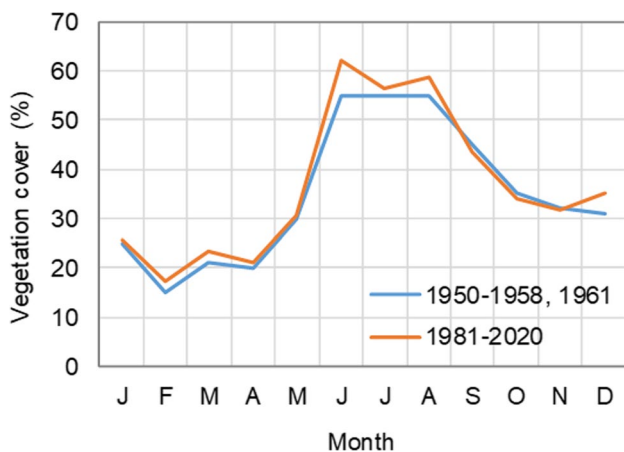


Fig. 3 Comparison of the mean monthly vegetation cover in the Bradano River Basin, estimated in the calibration years (1950–1958 and 1961) and determined from the Normalized Difference Vegetation Index for the period 1981–2020

1961. It is worth noting that these values are slightly lower than those observed from 1981 to 2020, indicating a recent shift towards higher values in vegetation cover (Fig. 3). This shift is attributed to the influence of higher atmospheric temperatures and increased CO_2 concentrations, which have stimulated Mediterranean vegetation growth (e.g. Osborne et al. 2000).

Figure 4A reports the regression results (black line) of the calibrated model, Eq. (1), for 120 net erosion data-points (blank circles falling out of bounds showing 95% prediction limits for new observations—in light pink—were not considered), where negligible departures of the data-points from the 1:1 red line are observed. The observed monthly values vary between 0 and $927 \text{ Mg km}^{-2} \text{ month}^{-1}$. The latter occurred in November 1959, when the annals of the former Hydrographic and Mareographic National Service registered a daily maximum rainfall equal to 116 mm d^{-1} with a cloudburst rainfall of 53 mm hr^{-1} . Figure 4B shows a distribution of the residuals compatible with a Gaussian pattern, indicating a free-skewed errors' distribution. The mean values of the predicted and observed values are not significantly different (pairwise Student-t $p = 0.95$). As the p -value of the Durbin–Watson ($DW = 1.73$) is greater than 0.05 ($p = 0.86$), there is no indication of serial autocorrelation in the residuals.

The R^2 -statistic indicates that the $\text{REDEM}_{(\text{BRB})}$ explained 87% of net erosion variability. The mean absolute error (MAE), used to quantify the amount of error, was equal to $18 \text{ Mg km}^{-2} \text{ month}^{-1}$, which is lower than the standard deviation of the residuals ($27 \text{ Mg km}^{-2} \text{ month}^{-1}$). The Nash–Sutcliffe efficiency (EF), equal to 0.85, also indicates narrow parameter uncertainty. With the calibration dataset capturing a wide variability of net erosion values, the satisfactory model performance obtained (according to an array of performance metrics and test statistics) supports the robustness of the model against contrasting situations.

In determining whether the $\text{REDEM}_{(\text{BRB})}$ can be simplified, we have fitted a multiple linear regression model to describe the relationship between net erosion and the four independent variables R_s , R_Q , SDR and VCP of Eq. (1). The highest p -value ($p = 0.0093$), belonging to SDR, indicates that even this term is statistically significant, and that Eq. (1) cannot be simplified further, resulting a stable, interpretable and generally useful model (Royston and Sauerbrei 2008).

In order to evaluate the time-scale invariance of the model, we have also aggregated net erosion on annual basis. Year-to-year fluctuations of actual net erosion values were largely reproduced by the time-integration of $\text{REDEM}_{(\text{BRB})}$ for all the years available (Fig. 4C). The values are in agreement ($R^2 = 0.91$ and $\text{MAE} = 60 \text{ Mg km}^{-2} \text{ yr}^{-1}$) and indicate the suitability of the annually integrated model for long-term assessments (standard deviation of the residuals equal to $89 \text{ Mg km}^{-2} \text{ yr}^{-1}$). The ability of the model to reproduce

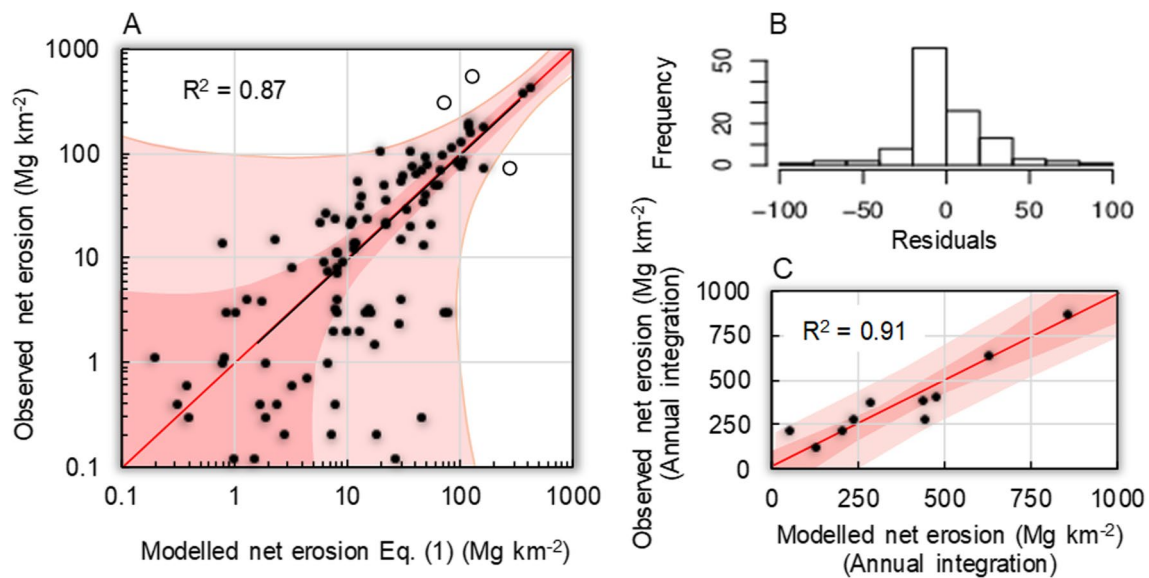


Fig. 4 **A** Scatterplot of observed experimentally determined (observed) monthly net erosion (NE) at the outlet of Bradano River Basin in the years 1950–1958 and 1961, and data modelled with Eq. (1). The graph includes the regression line (black line), the 1:1 identity line (red line), the prediction limits for the new observations at 90% (area coloured in deep pink) and 95% (area coloured in light pink) confidence (out of which the only outlier value is marked as an empty circle and not considered for model calibration). Units are in $\text{Mg km}^{-2} \text{ month}^{-1}$; **B** Residuals between actual and modelled net erosion; **C** Scatterplot of observed and modelled values of integrated

net erosion on an annual scale ($\text{Mg km}^{-2} \text{ yr}^{-1}$), with 1:1 identity line and associated confidence limits. The data used to generate the graphs of this figure were derived from the Regional Agency for Environmental Protection of Basilicata (ARPAB, Civil Protection Functional Centre, <http://centrofunzionalebasilicata.it>) and the former Hydrographic and Mareographic National Service for the years 1950–1958 and 1961 (Annals project 1957–1972, <https://www.isprambiente.gov.it/it/progetti/cartella-progetti-in-corso/acque-interne-e-marino-costiere-1/progetti-conclusi/progetto-annali>)

year-to-year fluctuations and generate accurate estimates of annual net erosion reinforces its reliability for long-term assessments. By demonstrating the time-scale invariance of the model, we establish its applicability in studying the complex dynamics of sediment yield over extended periods.

However, due to the lack of direct measurements, validation of the soil erosion estimates was also carried out by testing the predictive ability of the model to estimate the mean annual silting of the reservoir. In particular, $\text{REDEM}_{(\text{BRB})}$ estimates were compared to the sediment trapping data (dam silting) of the sub-basin subtended by the San Giuliano dam ($\sim 1669 \text{ km}^2$, i.e. 55% of the entire Bradano basin; Fig. 1B, light brown area), as supplied by the interregional authority responsible for its management for the period 1977–2000 (Spilotro et al. 2010). The comparison indicates that $\text{REDEM}_{(\text{BRB})}$ estimates ($316 \text{ Mg km}^{-2} \text{ yr}^{-1}$) can reliably quantify the amount of sediment yield at the mouth of Bradano River (silting at San Giuliano dam of $350 \text{ Mg km}^{-2} \text{ yr}^{-1}$). These features increase the robustness of this study, especially with regard to modelling, didactic simplicity and the environmental support role of the investigated landforms, despite its limitations. For instance, we do not have a way to validate the monthly values of the vegetation cover percentage until 1980. We obtained a mean annual vegetation cover of $\sim 35\%$, which is reflected in published

literature (e.g. Mancino 2002; Fuccella et al. 2010), and the estimated monthly percentages of vegetation cover may not reflect the phenology of the arable crops at the scale of the basin. In fact, at this spatial unit, wooded areas coexist with agricultural and vegetable crops. Specifically to our study area, vegetable crops grown in coastal areas require preparatory tillage in spring, which may explain a more limited extension of the vegetation cover in April than winter months. Then, the factors limiting vegetation dynamics vary according to the type of stand characteristics of mountain and Mediterranean biomes. Our understanding is that for vegetation located in warm areas, a temperature increase, a decrease in soil water availability, or a combination of both, is expected to reduce vegetation cover in spring. However, atmospheric and soil effects are difficult to assess in order to understand variations in vegetation dynamics, due to the complex interactions between the water regime and soil nutrition, which act in conjunction with the thermal and precipitation regimes (e.g. Piedallu et al. 2019). A posteriori, the satisfactory evaluation of the model (including the indirect evaluation against dam sediments) is a clue that our calibrated values of the vegetation cover percentage reliably reflect the monthly distribution of the vegetation cover.

3.2 Scaling of the temporal and spatial domains

In relatively small mountain basins, geomorphological processes are characterised by nonlinear interactions between climate, land surface and fluvial responses at different spatial and temporal scales. For instance, sediment transport dynamics are nonlinear, as they can be strongly influenced by increased sediment availability after extreme events, such as downpours and floods, and by the complex dynamics of activation of sediment sources with different degrees of connectivity to the drainage at the basin scale (Rainato et al. 2017).

A time-complexity approach in basin hydrological models must take into account the integration of fast-moving processes, such as the partitioning of precipitation into rain-splash and runoff (Mulligan and Wainwright 2004). Hydrological models are sensitive to the time step of the simulation, and then, in the representation of rainfall erosivity, only an indicator of the maximum hourly rainfall per month was taken, Eq. (2), to limit the large errors that can occur when aggregating intensity calculations in smaller steps. In this way, Eq. (2) is appropriate to account for the large variability from month to month, and between the same months in different years, in the amount of energy released in 1 to 24 h.

When the gross erosion has almost entirely originated, overland flow starts to prevail over splash erosion and the soil delivery ratio starts to detach the portion of the gross erosion that the tributaries introduce into the main hydrographic network until the outlet of the basin. It is observed that net erosion represents 68% of the eroded soil in the basin. Of the three relationships of R_s , R_Q and net erosion, R_s has a higher correlation with net erosion.

As Mulligan and Wainwright (2004) pointed out, the hydrological processes illustrated above are strongly dominated by the spatial connectivity of runoff-producing

elements. One attempt to incorporate upscaling in our model has been to account for both the VCP in the exponent of Eq. (1) and the SDR in Eq. (4).

The SDR has been modelled separately in a dynamic and hierarchical way based on the ratio between the runoff indicator (R_Q) and rainfall (p). In turn, the scaling of the SDR can be described as a simple power law of the linear regression of this ratio (Mandelbrot 1982), and be sufficient to capture basin-wide behaviour. It denotes the interaction between hillslope and channel in terms of runoff and sediment-delivery rates in a given month. The basin-scale multi-year mean SDR value estimated from Eq. (4) was equal to 0.68, close to the experimental value of 0.65 (Spilatro et al. 2010), thus obtaining a reliable quantification of the sediment. These values are consistent with the low slope of the basin.

3.3 Model application: seasonal and long-term erosion patterns

For the BRB, the results obtained over the long-term of 70 years (1950–2020) of modelling, net erosion exhibit a value of about $366 \pm 291 \text{ Mg km}^{-2} \text{ yr}^{-1}$. The years with net erosion around 1000 Mg km^{-2} occurred in 1954, 1959, 1972, 1979 and 1994 with 939, 1103, 1181, 932 and 938 Mg km^{-2} , respectively. From the annual standard deviation ($262 \text{ Mg km}^{-2} \text{ yr}^{-1}$), it is evident that there is a large inter-annual variability. A significant variation is also present in sediment transport on a monthly scale: in winter, the higher rate of annual sediment amount is delivered (39%), while 37% is delivered in autumn, and about 21% and 3%, in spring and summer, respectively. This is consistent with the soil types in the BRB, as the presence of arable land with seasonal cereal crops is more affected by erosion during the months without vegetation (Aiello et al. 2015).

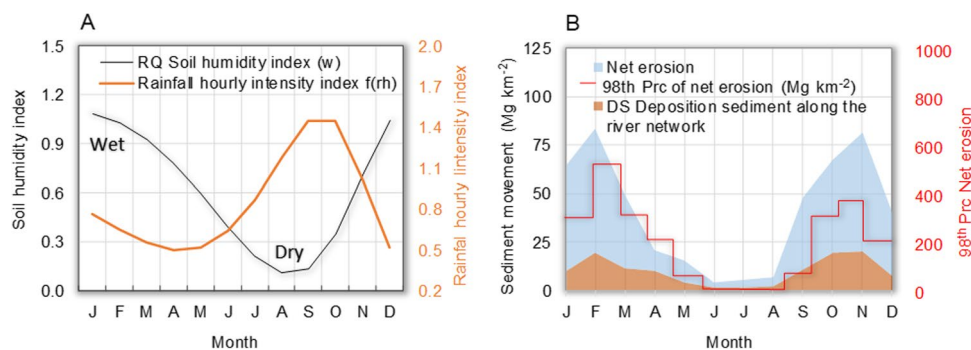


Fig. 5 **A** Monthly means of soil humidity index (black curve) and rainfall hourly intensity index (orange curve), and **B** eroded sediment balance for the Bradano River Basin averaged over the period 1950–2020 estimated with Eq. (1) and Eq. (7). In **B**, the red curve shows the 98th percentile (Prc) of net erosion. The data used to generate the graphs were derived from the Regional Agency for Environmental

Protection of Basilicata (ARPAB, Civil Protection Functional Centre, <http://centrofunzionalebasilicata.it>) and the former Hydrographic and Mareographic National Service for the years 1950–1958 and 1961 (Annals project 1957–1972, <https://www.isprambiente.gov.it/progetti/cartella-progetti-in-corso/acque-interne-e-marino-costiere-1/progetti-conclusi/progetto-annali>)

In this way, the rationale behind Eq. (1) is that two main processes are relevant to produce net erosion in the BRB: the power of rainfall through erosive-storm events, Eq. (2), and the transport capacity of eroded material through runoff, Eq. (3). In summer and early autumn, the erosive-storm factor operates mainly on a local scale from raindrop splash erosive forces, when the hourly rainfall intensity is higher (Fig. 5A, red line).

At this scale, storms cannot always carry sediment to the basin outlet, redistributing a larger ratio of sediment across the sub-basins. In the following stages, the gradual increase in the runoff rate in autumn and the moderate intensity of rainfall lead to a sharp increase in the runoff rate. During this period, cultivated land is active and subject to greater erosion risk. Long-lasting duration of winter and spring rains are usually associated with synoptic weather systems (Hawcroft et al. 2012), with decreasing rainfall intensity compared to the previous period and a sequence of storms which, however, favours rilling and thus increased soil erosion. In this case, runoff-erosion is added to splash-erosion, and can act even under moderate rainfall conditions, since the soil is well wetted (Fig. 5A, black line), and then more sediment is delivered to main drainage network and in turn to the basin outlet (Fig. 5B, blue band).

In contrast to driving factors, vegetation exerts basin-wide soil erosion control by dissipating the energy of rainfall (Ribolzi et al. 2017). In this way, vegetation patches trap sediment, particularly in summer and early autumn, playing an erosion-limiting role in about 50% along the BRB's main stream network (Fig. 5B, brown band), compared to 30% for other seasons. This seasonality may also be representative

of gross erosion that is trapped, like re-sedimentation, from the landscape before the eroded soil reaches the main river for delivery to the dam (with a quite high roughness coefficient, ~ 0.1 , Scarpino et al. 2018). Figure 5B (red curve, right y-axis) also shows the seasonal pattern of the 98th percentile of net erosion, which indicates rates five to ten times higher than the respective mean values (blue band, left y-axis), in winter, spring and autumn. This suggests that the extreme events, with return periods of about 50 years, can represent a damaging phenomenon in soil erosion processes. However, the decrease of net erosion does not occur in a linear, gradual trend (Fig. 6, black line) but, as shown by the change-point detected in 1986 by the Mann-Whitney-Pettit test ($p < 0.01$), by a sudden shift that divides the time-series in two distinct segments: 1950–1986 and 1987–2020 (red arrow). According to this change-point, the first period is affected by an areal mean sediment loss of $458 \text{ Mg ha}^{-2} \text{ yr}^{-1}$ (± 334 standard deviation), compared to $266 \text{ Mg ha}^{-2} \text{ yr}^{-1}$ (± 198 standard deviation) in the second period. For both of these periods, the values of terrigenous input at river mouths clearly reflect the characteristics of climate conditions and vegetation cover, and secondarily of soil erodibility, highlighting in particular the considerable role in limiting sediment transport played by man-made and natural landscape elements. As net erosion decreases, gross erosion declines (Mann–Kendall test $p = 0.02$), but at a higher rate (data not shown), since net erosion is also influenced by a reduction of the soil delivery ratio. Considering the annual time-series of sediment loss by severity classes, it can be seen that in $\sim 63\%$ and $\sim 27\%$ of the years the eroded material was above the tolerable annual

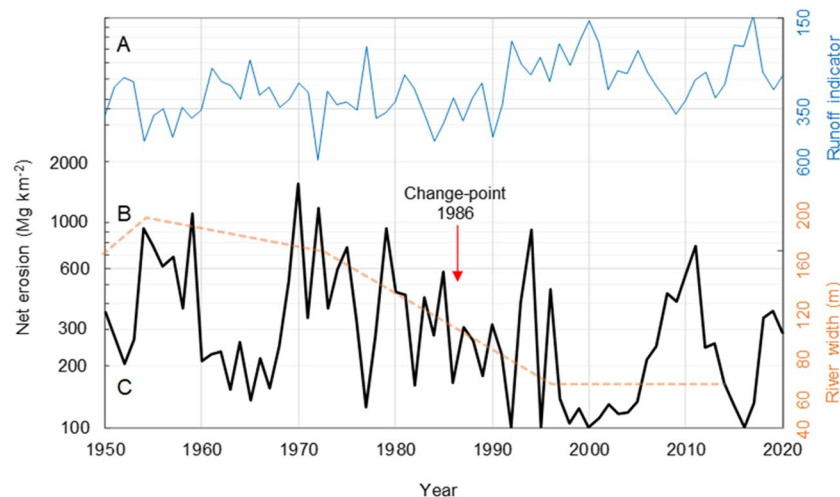


Fig. 6 **A** Temporal evolution of erosivity indicator associated more to runoff erosion for the Bradano River Basin during the period 1950–2020 (blue line); **B** Temporal trend of river width (m) of Basento Up (orange dashed line); and **C** Annual sediment loss (Mg km^{-2}) resulting from Eq. (1) (black line). Y-axis of net erosion and runoff

indicator (inverted axis) are in log-scale. The data used to generate the graphs were derived from the Regional Agency for Environmental Protection of Basilicata (ARPAB, Civil Protection Functional Centre, <http://centrofunzionalebasilicata.it>) and de Musso et al. (2020)

rates of 300 and 600 Mg km⁻² yr⁻¹ for poorly developed (< 0.5 m depth) and well developed (> 1 m depth) soils, respectively (OECD 2001).

In the long-term, the rainfall erosivity indicator, which is more associated with runoff erosion, appears to have affected the trend of sediment loss, especially after the change-point in 1986 (Fig. 6A, blue line), when this variable declined significantly (Mann–Kendall test: $S = -725$, $Z = 3.59$, $p \sim 0.00$). Although there is a possibility that the change-point detected in 1986 is related to the change of methodology in determining vegetation cover percentage (after 1980), this long-term decline in net erosion is consistent with the decrease in the width of the Basento Up channel (a river southwest of the Bradano River) in the period 1950–1996 and a flattening after that date (Fig. 6B, orange dashed line; de Musso et al. 2020).

According to de Musso et al. (2020), the Basento River channel narrowed strongly during the 20th century, similar to other Italian rivers like the Bradano River, with the strongest phase from the 1950s to the 1990s (with a variation in width from -30 to -80%).

Periodic oscillations also occur, consistent with the fluctuating pattern of net erosion, when net erosion remains stable and high for almost the first four decades of the time-series, when continuous inter-annual oscillations attest to erosion rates above the critical sediment loss (Fig. 6C, black line).

The decade of the 1950s is characterised by very high rates of sediment loss, as confirmed by the Italian historian Emilio Sereni (1907–1977), who considered indiscriminate deforestation to be the main cause of abnormal sediment production (Sereni 1961, p. 473):

“... quale è riflesso nella degradazione dei terreni montani, di conseguenza di inconsulti disboscamenti [...] e di una mancata politica di difesa del suolo, il cui aggravato difetto con particolare pericolosità si ripercorrevano in quegli anni anche al piano, con la frequenza e l'irruenza di nefaste alluvioni.”

“... which is reflected in the degradation of mountain soils, as a consequence of rash deforestation [...] and a lack of soil defence policy, whose aggravated defect with particular danger was traced in those years also on the plain, with the frequency and impetuosity of harmful floods.”

Subsequently, we find a group of years after 1970 which show considerable erosion rates and are among the highest in the time-series. In January 1972, for instance, the BRB was affected by exceptionally heavy rainfall, which lasted 10 days. According to Manfreda et al. (2015), the mean amount of rainfall in the lower part of the basin (Matera) was ~ 200 mm d⁻¹, with daily peaks of 310 mm in Calciano (40° 35' N, 16° 12' E) and 305 mm in Stigliano (40° 24' N, 16° 14' E). Inhabited centres were seriously damaged,

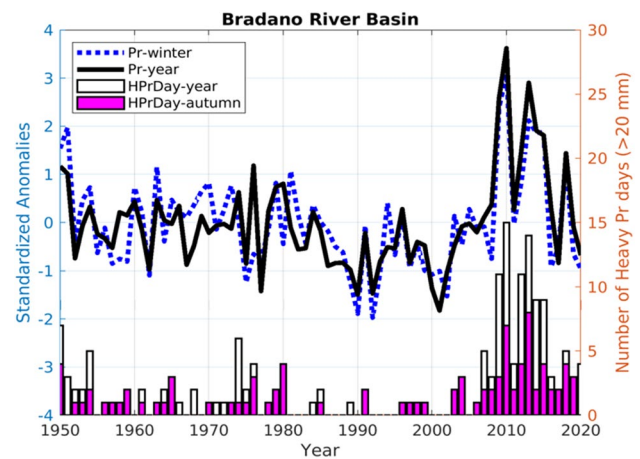


Fig. 7 Left y-axis: time-series evolution of standardized winter (December–February) and annual precipitation anomalies (mm per standard deviation) averaged over the area (40–41° N, 15°–17° E). Anomalies were calculated by subtracting their corresponding long-term annual or seasonal mean (1950–2020) from the time-series. Then, they were divided by their standard deviation. Right y-axis: number of days per year and per autumn (September–November) season when the mean areal precipitation is greater than 20 mm. The precipitation data used to generate the graph were derived from E-OBS v23.1e gridded dataset (https://surfobs.climate.copernicus.eu/dataaccess/access_eobs.php#datafiles) via Climate Explorer

roads and railways were disrupted, and the countryside was flooded by the overflow of the Basento and Cavone rivers (Manfreda et al. 2015). In Montalbano Jonico (40° 17' N, 16° 34' E), the rains triggered a landslide that threatened several houses. After the 1980s, the simulated erosion rates underwent a remarkable pattern-change and decline, characterised by long period of drought interrupted by small groups of years with high erosion rates, often above the tolerance threshold of 300 Mg km⁻² yr⁻¹ for shallow soils (Fig. 6C, black line). This is in line with the observed climate anomalies (Fig. 7), as these years have seen a sharp reduction in the amount of rainfall during the winter period and, consequently, an increase in aridity that has triggered land degradation processes in the southeast of the basin (Canora et al. 2015).

Also, during the last erosion peak around 2012, two exceptional rainfall events were observed. The south-eastern part of the Basilicata region, including the BRB municipalities, was the most affected by the rainstorms. The maximum amount of rainfall was recorded in the territory of Tursi (province of Matera in the southeast of the basin), where 152 mm of rain fell in 24 h. During the events of 5 and 7 October 2013, which affected the province of Matera, severe and widespread damage was observed in several parts of the province, causing the Bradano River to flood (Manfreda et al. 2015). This indicates that the regulation of soil and water conservation

measures on the spatio-temporal scale effects of the rainstorm-erosion processes in the BRB is at an unstable equilibrium, where events close to moderate-extreme storms can easily determine unsustainable conditions in soil loss in a long-term decline picture. This is the case of the period 2000–2020, when extreme autumn precipitation events and winter overland flow present higher values (Fig. 7). However, human intervention (e.g. channelization, arable land contraction) and the increase of natural vegetation appear to produce a counteracting effect (Romano and Cozzi 2007). This is also in agreement with the decrease in landslides and floods in the period 1951–2000 found by Clarke and Rendell (2006) for the Basilicata region. It can also be assumed that the luxury of vegetation in recent years has been increased by the rise in average temperatures in all seasons of the year (Diodato and Bellocchi 2008). In this way, landscape changes have contributed to reducing the risk of soil erosion due to the positive effects of vegetation cover in confining the energy of precipitation. This decline in soil erosion hazard was also confirmed by Mancino et al. (2016), for the period 1990–2010, for which forests increased by 5.6% as an indirect response to land abandonment.

4 Conclusions and perspectives

4.1 Key findings and insights

The study focused on reconstructing sediment loss in the Bradano River Basin (BRB) from 1950 to 2020 to evaluate erosional processes in Mediterranean environments. By employing the REDEM_(BRB) model, which utilises climatic and vegetation data, we were able to quantitatively assess net erosion. The model's performance was satisfactory, effectively capturing inter-annual variability and seasonal erosion patterns. Notably, vegetation emerged as a critical factor in controlling soil erosion by dissipating rainfall energy and trapping sediment, particularly during summer and early autumn. The study's findings have practical implications for land and water management, offering valuable insights for erosion control measures and reservoir management in the BRB. The identification of a change-point in erosion dynamics in c. 1986 emphasizes a shift in erosion dynamics, underscoring the importance of continuous monitoring and adaptive management strategies. Furthermore, long-term assessments employing the annually integrated model can provide valuable information for watershed management and decision-making. To improve the model's predictive capabilities, future research should focus on refining it

by incorporating additional variables such as land use changes, climate change projections and soil conservation practices. Rigorous monitoring and validation efforts under different scenarios are also necessary to assess the model's performance accurately. Additionally, applying the model to other river basins with similar characteristics can help evaluate its transferability and generalize its findings, extending its applicability beyond the BRB.

4.2 Significance of the study and recommendations

The significance of this study extends to supporting the implementation of landscape planning guidelines in Basilicata, specifically the “Guidelines for integrated landscape planning in Basilicata” (*Linee guida per la progettazione integrata del paesaggio della Basilicata*). These guidelines, based on the principles of the European Landscape Convention (Giambersio and Menchise 2010), provide a framework for landscape planning methodologies at the regional level, defining a cognitive framework for the regional landscape and offering guidance for landscape recognition and design. By developing the REDEM_(BRB) model and gaining insights into erosion patterns in the BRB, this study provides valuable information that can support the implementation of these guidelines. For future research, it is recommended to focus on incorporating additional variables such as land use changes, climate change projections and soil conservation practices to enhance the model's predictive capabilities. Rigorous monitoring and validation efforts under different scenarios are necessary to validate the model's estimates and assess its performance. Furthermore, applying the model to other river basins with similar characteristics can help evaluate its transferability and generalize its findings, expanding its applicability beyond the BRB. These advancements also set the stage for informed decision-making, sustainable land and water management practices, and the preservation of ecological processes (Jiménez-Alfaro et al. 2020).

Supplementary Information The online version contains supplementary material available at <https://doi.org/10.1007/s00704-023-04662-3>.

Author contribution N. D. conceived the study, performed most of the analysis and drafted the manuscript with G. B., who wrote the final manuscript. P. B. and I. G. performed complementary analyses and contributed to the scientific discussions.

Funding Open Access funding provided thanks to the CRUE-CSIC agreement with Springer Nature. The authors performed this research as an investigator-driven study without financial support.

Data availability Mean rate of soil loss in central and southern Europe: European Soil Data Centre (ESDAC, <https://esdac.jrc.ec.europa.eu/themes/rainfall-erosivity-europe>). Hydrographic network of the Bradano River Basin: Italian Institute for Environmental Protection and Research (<http://sgi2.isprambiente.it/viewersgi2>). Rainfall data from Irsina station: SCIA (Sistema nazionale per l'elaborazione e diffusione

di dati climatici) dataset (<http://www.scia.isprambiente.it>). Annual rainfall erosivity, monthly soil humidity, rainfall hourly intensity index and runoff erosion across the Bradano River Basin: Capolongo et al. (2008) and European Soil Data Centre (ESDAC, <https://esdac.jrc.ec.europa.eu/themes/rainfall-erosivity-europe>). Observed net erosion in the Bradano River Basin: Regional Agency for Environmental Protection of Basilicata (ARPAB, Civil Protection Functional Centre, <http://centrofunzionalebasilicata.it>) and the former Hydrographic and Mareographic National Service for the years 1950–1958 and 1961 (Annals project 1957–1972, <https://www.isprambiente.gov.it/it/progetti/carte-lla-progetti-in-corso/acque-interne-e-marino-costiere-1/progetti-conclusi/progetto-annali>). Temporal trend of river width of Basento Up: de Musso et al. (2020). Daily precipitation for the Bradano River Basin for the period 1950–2020: E-OBS daily precipitation data: E-OBS v23.1e (https://surfobs.climate.copernicus.eu/dataaccess/access_eobs.php#datafiles). Normalized Difference Vegetation Index (NDVI) data from National Oceanic and Atmospheric Administration Climate Data Record (Vermote 2019), provided by Climate Explorer (https://climatexp.knmi.nl/select.cgi?id=someone@somewhere&field=ndvi_noaa_01). The data used for model calibration (1950–1961) and generated with the model (1950–2020) are available as supplementary material.

Code availability Codes can be available upon request to the authors.

Declarations

Competing interests The authors declare no competing interests.

Open Access This article is licensed under a Creative Commons Attribution 4.0 International License, which permits use, sharing, adaptation, distribution and reproduction in any medium or format, as long as you give appropriate credit to the original author(s) and the source, provide a link to the Creative Commons licence, and indicate if changes were made. The images or other third party material in this article are included in the article's Creative Commons licence, unless indicated otherwise in a credit line to the material. If material is not included in the article's Creative Commons licence and your intended use is not permitted by statutory regulation or exceeds the permitted use, you will need to obtain permission directly from the copyright holder. To view a copy of this licence, visit <http://creativecommons.org/licenses/by/4.0/>.

References

- Aiello A, Adamo M, Canora F (2015) Remote sensing and GIS to assess soil erosion with RUSLE3D and USPED at river basin scale in southern Italy. *Catena* 131:174–185. <https://doi.org/10.1016/j.catena.2015.04.003>
- Arabameri A, Sadhasivam N, Turabieh H et al (2021) Credal decision tree based novel ensemble models for spatial assessment of gully erosion and sustainable management. *Sci Rep* 11:3147. <https://doi.org/10.1038/s41598-021-82527-3>
- Arnold JG, Williams JR, Maidment DA (1995) A continuous time water and sediment routing model for large basins. *J Hydraulic Div ASCE* 121:171–183. [https://doi.org/10.1061/\(ASCE\)0733-9429\(1995\)121:2\(171\)](https://doi.org/10.1061/(ASCE)0733-9429(1995)121:2(171))
- Borrelli P, Van Oost K, Meusburger K et al (2018) A step towards a holistic assessment of soil degradation in Europe: coupling on-site erosion with sediment transfer and carbon fluxes. *Environ Res* 161:291–298. <https://doi.org/10.1016/j.envres.2017.11.009>
- Borrelli P, Alewell C, Álvarez P et al (2021) Soil erosion modelling: a global review and statistical analysis. *Sci Tot Env* 780:146494. <https://doi.org/10.1016/j.scitotenv.2021.146494>
- Browning TN, Sawyer DE (2021) Vulnerability to watershed erosion and coastal deposition in the tropics. *Sci Rep* 11:885. <https://doi.org/10.1038/s41598-020-79402-y>
- Canora F, D'Angella A, Aiello A (2015) Quantitative assessment of the sensitivity to desertification in the Bradano River basin (Basilicata, southern Italy). *J Maps* 11(5):745–759. <https://doi.org/10.1080/174456472014980857>
- Capolongo D, Diodato N, Mannaerts CM et al (2008) Analyzing temporal changes in climate erosivity using a simplified rainfall erosivity model in Basilicata. *J Hydrol* 356:119–130. <https://doi.org/10.1016/j.jhydrol.2008.04.002>
- Cardinali F (1828) *Del moto e della misura dell'acqua* – di Leonardo da Vinci Libro VI (pp 450). Italy (in Italian), Bologna
- Clarke ML, Rendell HM (2006) Hindcasting extreme events: the occurrence and expression of damaging floods and landslides in Southern Italy. *Land Degrad Dev* 17:365–380. <https://doi.org/10.1002/ldr743>
- Cornes RC, van der Schrier G, van den Besselaar EJM, Jones PD (2018) An ensemble version of the E-OBS temperature and precipitation data sets. *J Geophys Res* 123:9391–9409. <https://doi.org/10.1029/2017JD028200>
- Cudahy T, Caccetta M, Thomas M et al (2016) Satellite-derived mineral mapping and monitoring of weathering, deposition and erosion. *Sci Rep* 6:23702. <https://doi.org/10.1038/srep23702>
- de Vente J, Poesen J (2005) Predicting soil erosion and sediment yield at the basin scale: Scale issues and semi-quantitative models. *Earth-Sci Rev* 71:95–125. <https://doi.org/10.1016/j.earscirev.2005.02.002>
- de Musso NM, Capolongo D, Caldara M et al (2020) Channel changes and controlling factors over the past 150 years in the Basento River (Southern Italy). *Water* 12:307. <https://doi.org/10.3390/w12010307>
- de Vente J, Poesen J, Verstraeten G et al (2013) Predicting soil erosion and sediment yield at regional scales: Where do we stand? *Earth-Sci Rev* 127:16–29. <https://doi.org/10.1016/j.earscirev.2013.08.014>
- Diodato N, Aronica G (2014) Finding simplicity in storm erosivity modelling. In: Diodato N, Bellocchi G (eds) *Storminess and environmental change: climate forcing and response in the Mediterranean region*. Springer, Dordrecht, The Netherlands, pp 53–64
- Diodato N, Bellocchi G (2007a) Estimating monthly (R)USLE climate input in a Mediterranean region using limited data. *J Hydrol* 345:224–236. <https://doi.org/10.1016/j.jhydrol.2007a08008>
- Diodato N, Bellocchi G (2007b) Modeling reference evapotranspiration over complex terrains from minimum climatological data. *Water Resour Res* 43:W05444. <https://doi.org/10.1029/2006WR005405>
- Diodato N, Bellocchi G (2008) Modelling NDVI responses to climate variability in Mediterranean terrestrial ecosystem. *Env Monit Assess* 44:147–159. <https://doi.org/10.1007/s10661-007-9964-z>
- Diodato N, Bellocchi G (2019) Reconstruction of seasonal net erosion in a Mediterranean landscape (Alento River Basin, Southern Italy) over the past five decades. *Water* 11:2306. <https://doi.org/10.3390/w11112306>
- Diodato N, Gericke A, Bellocchi G (2012) Modelling the inter-annual variability of sediment yields: A case study for the upper Lech River. *Catena* 97:12–19. <https://doi.org/10.1016/j.catena.2012.04.013>
- Diodato N, de Vente J, Bellocchi G et al (2015) Estimating long-term sediment export using a seasonal rainfall-dependent hydrological model in the Glonn River basin, Germany. *Geomorphology* 228:628–636. <https://doi.org/10.1016/j.geomorph.2014.10.011>

- Diodato N, Guerriero L, Bellocchi G (2017) Modeling and upscaling plot-scale soil erosion under Mediterranean climate variability. *Environments* 4:58. <https://doi.org/10.3390/environments4030058>
- Diodato N, Mao L, Borrelli P et al (2018) Climate-scale modelling of suspended sediment load in an Alpine catchment debris flow (Rio Cordon-northeastern Italy). *Geomorphology* 309:20–28. <https://doi.org/10.1016/j.geomorph.2018.02.026>
- Diodato N, Filizola N, Borrelli P, Panagos P, Bellocchi G (2020) The rise of climate-driven sediment discharge in the Amazonian River Basin. *Atmosphere* 11:208. <https://doi.org/10.3390/atmos11020208>
- Diodato N, Ljungqvist FC, Bellocchi G (2021) A millennium-long climate history of erosive storms across the Tiber River Basin, Italy, from 725 to 2019 CE. *Sci Rep* 11:20518. <https://doi.org/10.1038/s41598-021-99720-z>
- Diodato N, Ljungqvist FC, Bellocchi G (2021) Outcome of environmental change from historical sediment discharge in a Mediterranean fluvial basin, 1500–2019 CE. *Env Res Commun* 3:071002. <https://doi.org/10.1088/2515-7620/ac0b83>
- Diodato N, Fiorillo F, Rinaldi M, Bellocchi G (2022) Environmental drivers of dynamic soil erosion change in a Mediterranean fluvial landscape. *PLoS One* 17:e0262132. <https://doi.org/10.1371/journal.pone.0262132>
- Foster GR, Meyer LD, Onstad CA (1977) Runoff erosivity factor and variable slope length exponents for soil loss estimates. *Trans ASAE* 20:683–687. <https://doi.org/10.13031/2013.35628>
- Fuccella P, Labella A, Lavorano EM (2010) Note di storia sul paesaggio agrario della Basilicata tra XIX e XXI secolo. Calice Editore, Potenza, p 252 (in Italian)
- Gericke A, Venohr M (2012) Improving the estimation of erosion-related suspended solid yields in mountainous, non-alpine river catchments. *Environ Model Softw* 37:30–40. <https://doi.org/10.1016/j.envsoft.2012.04.008>
- Giambersio V, Menchise C (2010) La trasformazione del paesaggio agrario in Basilicata nel XX secolo. In: Fuccella P, Labella A, Lavorano EM (eds) Note di storia sul paesaggio agrario della Basilicata tra XIX e XXI secolo. Calice Editore, Potenza, pp 81–148 (in Italian)
- Gostelow TP, Del Prete M, Simoni A (1997) Slope instability in historic hilltop towns of Basilicata, southern Italy. *Q J Eng Geol Hydrogeol* 30:3–26. <https://doi.org/10.1144/GSL.QJEGH.1997.030.P1.02>
- Guo T, Srivastava A, Flanagan DC (2021) Improving and calibrating channel erosion simulation in the Water Erosion Prediction Project (WEPP) model. *J Environ Manage* 291:112616. <https://doi.org/10.1016/j.jenvman.2021.112616>
- Gupta S, Kumar S (2017) Simulating climate change impact on soil erosion using RUSLE model – A case study in a watershed of mid-Himalayan landscape. *J Earth Syst Sci* 126:43. <https://doi.org/10.1007/s12040-017-0823-1>
- Haan CT, Barfield BJ, Hayes JC (1994) Design hydrology and sedimentology for small catchments. Academic Press. <https://doi.org/10.1016/B978-0-08-057164-5.50002-5>
- Hawcroft MK, Shaffrey LC, Hodges KI, Dacre HF (2012) How much Northern Hemisphere precipitation is associated with extratropical cyclones? *Geophys Res Lett* 39:L24809. <https://doi.org/10.1029/2012GL053866>
- Hussainzada W, Lee HS (2022) Effect of an improved agricultural irrigation scheme with a hydraulic structure for crop cultivation in arid northern Afghanistan using the Soil and Water Assessment Tool (SWAT). *Sci Rep* 12:5186. <https://doi.org/10.1038/s41598-022-09318-2>
- Jiang Z, Su S, Jing C, Lin S, Fei X, Wu J (2012) Spatiotemporal dynamics of soil erosion risk for Anji County. *China Stoch Env Res Risk A* 26:751–763. <https://doi.org/10.1007/s00477-012-0590-0>
- Jiménez-Alfaro B, Frischie S, Stolz J et al (2020) Native plants for greening Mediterranean agroecosystems. *Nat Plants* 6:209–214. <https://doi.org/10.1038/s41477-020-0617-3>
- Kemp DB, Sadler PM, Vanacker V (2020) The human impact on North American erosion, sediment transfer, and storage in a geologic context. *Nat Commun* 11:6012. <https://doi.org/10.1038/s41467-020-19744-3>
- Kinnel PIA (2010) Event soil loss, runoff and the Universal Soil Loss Equation family of models: A review. *J Hydrol* 385:384–397. <https://doi.org/10.1016/j.jhydrol.2010.01.024>
- Labella A (2010) Il paesaggio agrario della Basilicata nella storiografia nazionale e regionale dell'ultimo ventennio. In: Fuccella P, Labella A, Lavorano EM (eds) Note di storia sul paesaggio agrario della Basilicata tra XIX e XXI secolo. Calice Editore, Potenza, pp 11–50 (in Italian)
- Lim KJ, Engel BA, Tang Z, Muthukrishnan S, Choi J, Kim K (2006) Effects of calibration on L-THIA GIS runoff and pollutant estimation. *J Environ Manage* 78:35–43. <https://doi.org/10.1016/j.jenvman.2005.03.014>
- Mancino G (2002) Rischio di erosione: telerilevamento e GIS per l'applicazione della Universal Soil Loss Equation (USLE). *Monti e Boschi* 5:29–36 (in Italian)
- Mancino G, Nolè A, Salvati L, Ferrara A (2016) In-between forest expansion and cropland decline: a revised USLE model for soil erosion risk under land-use change in a Mediterranean region. *Ecol Indic* 71:544–550. <https://doi.org/10.1016/j.ecolind.2016.07.040>
- Mandelbrot BB (1982) *The Fractal Geometry of Nature*. Freeman, New York, p 460
- Manfreda S, Sole A, De Costanzo G (2015) Le precipitazioni estreme in Basilicata. In: *Universosud Società Cooperativa* (ed) Università degli Studi della Basilicata, p 146 (in Italian)
- Merritt WS, Letcher RA, Jakeman AJ (2003) A review of erosion and sediment transport models. *Environ Model Softw* 18:761–799. [https://doi.org/10.1016/S1364-8152\(03\)00078-1](https://doi.org/10.1016/S1364-8152(03)00078-1)
- Mulligan M, Wainwright J (2004) Modelling and model building. In: Wainwright J, Mulligan M (eds) *Environmental Modelling: Finding Simplicity in Complexity*. John Wiley and Sons Ltd, Chichester, pp 7–73
- OECD (2001) Environmental indicators for agriculture methods and results vol 3. In: OECD (Ed), *Agriculture and food*, pp 409
- Osborne CP, Mitchell PL, Sheehy JE, Woodward FI (2000) Modelling the recent historical impacts of atmospheric CO₂ and climate change on Mediterranean vegetation. *Glob Change Biol* 6:445–458. <https://doi.org/10.1046/j.1365-2486.2000.00336.x>
- Panagos P, Borrelli P, Meusburger K et al (2017) Global rainfall erosivity assessment based on high-temporal resolution rainfall records. *Sci Rep* 7:4175. <https://doi.org/10.1038/s41598-017-04282-8>
- Panagos P, Ballabio C, Poesen J et al (2020) A soil erosion indicator for supporting agricultural, environmental and climate policies in the European Union. *Remote Sens* 12:1365. <https://doi.org/10.3390/rs12091365>
- Piedallu C, Chéret V, Denux JP et al (2019) Soil and climate differently impact NDVI patterns according to the season and the stand type. *Sci Total Environ* 651:2874–2885. <https://doi.org/10.1016/j.scitotenv.2018.10.052>
- Pilogallo A, Saganeiti L, Scorza F, Murgante B (2020) Soil ecosystem services and sediment production: the Basilicata Region case study. In: Gervasi O et al (eds) *Computational Science and Its Applications – ICCSA 2020, Lecture notes in computer science*, vol 12253, pp 421–435, Springer Nature, Switzerland. https://doi.org/10.1007/978-3-030-58814-4_30
- Pruski FF, Nearing MA (2002) Runoff and soil-loss responses to changes in precipitation: a computer simulation study. *J Soil Water Conserv* 57:7–16

- Quinton JN, Catt JA, Wood GA, Steer J (2006) Soil carbon losses by water erosion: experimentation and modeling at field and national scales in the UK. *Agric Ecosyst Environ* 112:87–102. <https://doi.org/10.1016/j.agee.2005.07.005>
- Rainato R, Mao L, García-Rama A et al (2017) Three decades of monitoring in the Rio Cordon instrumented basin: sediment budget and temporal trend of sediment yield. *J Geomorph* 291:45–56. <https://doi.org/10.1016/j.geomorph.2016.03.012>
- Ran L, Lu X, Fang N, Yang X (2018) Effective soil erosion control represents a significant net carbon sequestration. *Sci Rep* 8:12018. <https://doi.org/10.1038/s41598-018-30497-4>
- Renard KD, Foster GR, Weesies GA, Porter JP (1991) RUSLE-revised universal soil loss equation. *J Soil Water Conserv* 46:30–33
- Ribolzi O, Evrard O, Huon S et al (2017) From shifting cultivation to teak plantation: effect on overland flow and sediment yield in a montane tropical catchment. *Sci Rep* 7:3987. <https://doi.org/10.1038/s41598-017-04385-2>
- Romano S, Cozzi M (2007) Cambiamenti nell'uso del suolo: analisi e comparazione di mappe storiche e recenti. Il caso della Valle dell'Agri, Basilicata. *Italia Aestimum* 51:63–89 (in Italian)
- Royston P, Sauerbrei W (2008) Multivariable model - building: a pragmatic approach to regression analysis based on fractional polynomials for modelling continuous variables. John Wiley & Sons Ltd, Chichester, UK, p 303
- Scarpino S, Albano R, Cantisani A et al (2018) Multitemporal SAR data and 2D hydrodynamic model flood scenario dynamics assessment. *ISPRS Int J Geoinf* 7:105. <https://doi.org/10.3390/ijgi7030105>
- Sereni E (1961) Storia del paesaggio agrario Italiano Bari. Laterza, p 500 (in Italian)
- Shojaei S, Kalantari Z, Rodrigo-Comino J (2020) Prediction of factors affecting activation of soil erosion by mathematical modeling at pedon scale under laboratory conditions. *Sci Rep* 10:20163. <https://doi.org/10.1038/s41598-020-76926-1>
- Spilotro G, Canora F, Cicala A (2010) Attività antropica e variazioni del bacino sedimentario relativo alla costa Ionica della Basilicata. *Atti del Dipartimento di Strutture, Geotecnica e Geologia Applicata dell'Università della Basilicata* 2:1–18 (in Italian)
- Thomas MF (2001) Landscape sensitivity in time and space – an introduction. *CATENA* 42:83–98. [https://doi.org/10.1016/S0341-8162\(00\)00133-8](https://doi.org/10.1016/S0341-8162(00)00133-8)
- Thornes JB (1990) The interaction of erosional and vegetational dynamics in land degradation: spatial outcomes. In: Thornes JB (ed) *Vegetation and erosion: processes and environments*. Wiley, Chichester, UK, pp 41–55
- Toy TJ, Foster GR, Renard KG (2002) *Soil erosion; prediction, measurement, and control*. John Wiley & Sons, New York
- Van Rompaey AJ, Verstraeten G, Van Oost K, Govers G, Poesen J (2001) Modelling mean annual sediment yield using a distributed approach. *Earth Surf Proc Land* 26:1221–1236. <https://doi.org/10.1002/esp.275>
- Vermote E (2019) NOAA Climate Data Record (CDR) of AVHRR Normalized Difference Vegetation Index (NDVI), Version 5 NOAA National Centers for Environmental Information. <https://doi.org/10.7289/V5TM782M>
- Wischmeier WH, Smith DD (1965) Predicting rainfall erosion losses from cropland east of the Rocky Mountains: a guide for selection of practices for soil and water conservation. *Agricultural Handbook* 282:47
- Wischmeier WH, Smith DD (1978) *Predicting rainfall erosion losses: A guide to conservation planning*. U.S. Department of Agriculture, Agriculture Handbook No. 537, Washington, DC
- Zhang XF, Xu QX, Pei Y (2001) Preliminary research on the BP networks forecasting model of watershed runoff and sediment yielding. *Adv Water Sci* 12:17–22
- Zhang FB, Bai YJ, Xie LY et al (2017) Runoff and soil loss characteristics on loess slopes covered with aeolian sand layers of different thicknesses under simulated rainfall. *J Hydrol* 549:244–251. <https://doi.org/10.1016/j.jhydrol.2017.04.002>

Publisher's Note Springer Nature remains neutral with regard to jurisdictional claims in published maps and institutional affiliations.